

Heavy Quarks: lessons learned from HERA and Tevatron

Fredrick Olness,^{a*} Ingo Schienbein,^b

^aSouthern Methodist University, Dallas, TX 75275-0175 USA

^bLaboratoire de Physique Subatomique et de Cosmologie, Université Joseph Fourier Grenoble 1, CRNS/IN2P3, Institut National Polytechnique de Grenoble, 38026 Grenoble, France

We review some of the recent developments which have enabled the heavy quark mass to be incorporated into both the calculation of the hard-scattering cross section and the PDFs. We compare and contrast some of the schemes that have been used in recent global PDF analyses, and look at issues that arise when these calculations are extended to NNLO.

1. Introduction

The production of heavy quarks in high energy processes has become an increasingly important subject of study both theoretically and experimentally. The theory of heavy quark production in perturbative Quantum Chromodynamics (PQCD) is more challenging than that of light parton (jet) production because of the new physics issues brought about by the additional heavy quark mass scale. The correct theory must properly take into account the changing role of the heavy quark over the full kinematic range of the relevant process from the threshold region (where the quark behaves like a typical “heavy particle”) to the asymptotic region (where the same quark behaves effectively like a parton, similar to the well known light quarks $\{u, d, s\}$).

We review theoretical methods which have been advanced to improve existing QCD calculations of heavy quark production, and the impact on recent experimental results from HERA and the Tevatron.

The ACOT renormalization scheme provides a mechanism to incorporate the heavy quark mass into the theoretical calculation of heavy quark production both kinematically and dynamically. In 1998 Collins [1] extended the factorization theorem to address the case of heavy quarks; this work provided the theoretical foundation that allows us to reliably compute heavy quark processes

throughout the full kinematic realm.

1.1. NLO DIS calculation

Figure 1 displays characteristic Feynman graphics for the first few orders of DIS heavy quark production. If we consider the DIS production of heavy quarks at $\mathcal{O}(\alpha_S^1)$ this involves the LO $QV \rightarrow Q$ process and the NLO $gV \rightarrow Q\bar{Q}$ process.

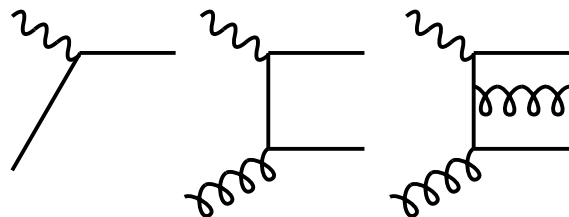


Figure 1. Characteristic Feynman graphs which contribute to DIS heavy quark production: a) the LO $\mathcal{O}(\alpha_S^0)$ quark-boson scattering $QV \rightarrow Q$, b) the NLO $\mathcal{O}(\alpha_S^1)$ gluon-boson scattering $gV \rightarrow Q\bar{Q}$, and c) the NNLO $\mathcal{O}(\alpha_S^2)$ boson-gluon scattering $gV \rightarrow gQ\bar{Q}$.

The key ingredient provided by the ACOT scheme is the subtraction term (SUB) which removes the “double counting” arising from the regions of phase space where the LO and NLO contributions overlap. Specifically, the subtraction

*Presented by Fred Olness

term is:

$$\sigma_{SUB} = f_g \otimes \tilde{P}_{g \rightarrow Q} \otimes \sigma_{QV \rightarrow Q} \quad .$$

σ_{SUB} represents a gluon emitted from a proton (f_g) which undergoes a collinear splitting to a heavy quark ($\tilde{P}_{g \rightarrow Q}$) convoluted with the LO quark-boson scattering $\sigma_{QV \rightarrow Q}$. Here, $\tilde{P}_{g \rightarrow Q}(x, \mu) = \frac{\alpha_s}{2\pi} \ln(\mu^2/m_c^2) P_{g \rightarrow c}(x)$ where $P_{g \rightarrow c}(x)$ is the usual \overline{MS} splitting kernel.

1.2. When do we need Heavy Quark PDFs

The novel ingredient in the above calculation is the inclusion of the heavy quark PDF contribution which resums logs of $\ln(\mu^2/m_Q^2)$. One can ask the question: When do we need to consider such terms? The answer is illustrated in Figure 2 where we compare the DGLAP evolved PDF $f_c(x, \mu)$ with the single splitting perturbative result.

The DGLAP PDF evolution sums a non-perturbative infinite tower of logs while the SUB contribution removes the perturbative single splitting component which is already included in the NLO contribution. Hence, at the PDF level the difference between the heavy quark DGLAP evolved PDF f_Q and the single-splitting perturbative \tilde{f}_Q will indicate the contribution of the higher order logs which are resummed into the heavy quark PDF. Here, we shall find it convenient to define $\tilde{f}_Q = f_g \otimes \tilde{P}_{g \rightarrow Q}$ which represents the PDF of a heavy quark Q generated from a single perturbative splitting.

For $\mu \sim m_Q$ we see that f_Q and \tilde{f}_Q match quite closely, whereas f_Q and \tilde{f}_Q differ significantly for μ values a few times m_Q . While the details will depend on the specific process, in general we find that for μ scales 3 to 5 times m_Q the terms resummed by the heavy quark PDF can be significant.

2. The ACOT Renormalization Scheme

2.1. Massive vs. Massless Evolution

Another useful result that arises from the proof of Collins [1] is that we can use mass-independent (massless) evolution kernels to evolve the heavy quark PDFs without any loss of accuracy as compared to a mass-dependent (massive) evolution

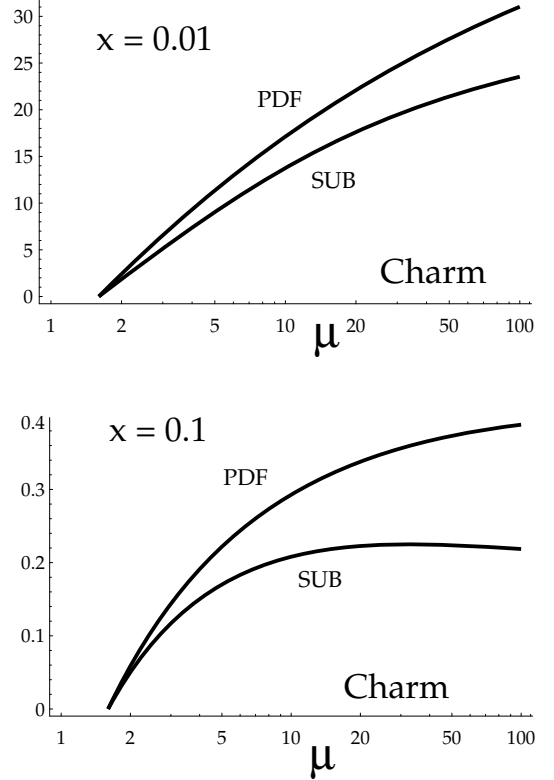


Figure 2. Comparison of the DGLAP evolved charm PDF $f_c(x, \mu)$ with the perturbatively computed single splitting (SUB) $\tilde{f}_c(x, \mu) = f_g(x, \mu) \otimes \tilde{P}_{g \rightarrow c}$ charm evolution vs. μ in GeV for two representative values of x .

kernel. [2]. Specifically, Collins demonstrated that consistent application of the formalism correctly resums the massive contributions up to higher-twist corrections $\mathcal{O}(\Lambda_{QCD}^2/Q^2)$ and that there are no errors of order $\mathcal{O}(m_Q^2/Q^2)$.

This result is illustrated in Figure 3 where we compare the results of a NLO DIS heavy quark production calculation using massless and massive DGLAP evolution kernels. In Fig. 3a) we see that while the choice of massive or massless kernels significantly changes the individual LO and SUB contributions, the difference $LO - SUB$ which contributes to the total ($TOT = LO -$

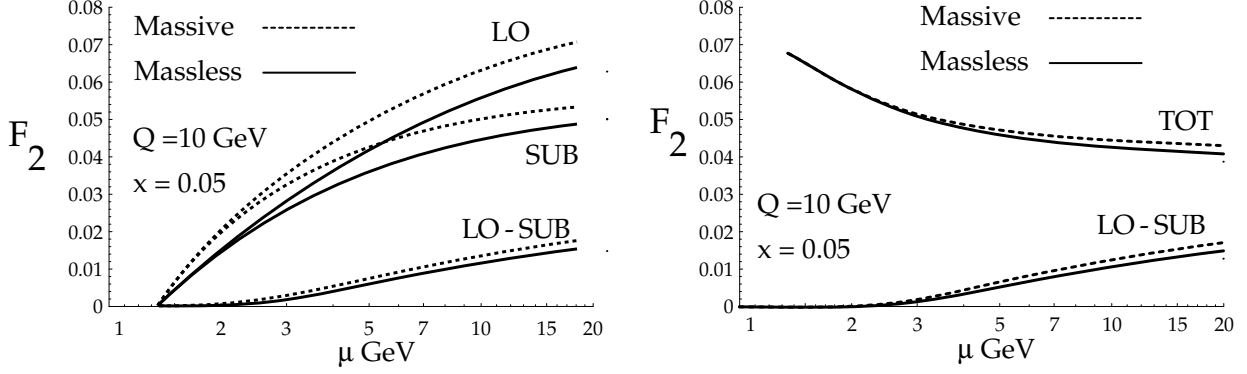


Figure 3. Comparison of heavy quark DIS structure function for mass-dependent (massive) and mass-independent (massless) evolution.

$SUB + NLO$) is minimal. This numerically verifies that the choice of massive or massless evolution kernels is purely a scheme choice which has no physical content.

While we see this result demonstrated numerically in Figure 3, the underlying reason for this result is closely related to the previous observations made regarding Figure 2. The LO result is given by $LO \sim f_Q \otimes \sigma_{Q \rightarrow Q}$ and the subtraction term is given by $SUB \sim f_g \otimes \tilde{P}_{g \rightarrow Q} \otimes \sigma_{Q \rightarrow Q}$. If we expand the DGLAP equation for f_Q in the region $\mu \sim m_Q$ we find $f_Q \sim f_g \otimes \tilde{P}_{g \rightarrow Q} + \mathcal{O}(\alpha_s^2)$; thus, we have $LO \sim f_g \otimes \tilde{P}_{g \rightarrow Q} \otimes \sigma_{Q \rightarrow Q} + \mathcal{O}(\alpha_s^2)$. We observe that while LO and SUB individually depend on the specific splitting kernels, the combination $LO - SUB$ is insensitive to whether we use the massive or massless kernel.²

Therefore, we conclude that so long as the splitting kernels $P_{a \rightarrow b}$ are matched between the DGLAP evolution and the definition of the subtractions (SUB), the choice of a massive or massless DGLAP evolution kernel was purely a choice of scheme and the physical results are invariant.

2.2. S-ACOT

In a complementary application, it was observed that the heavy quark mass could be set to zero in certain pieces of the hard scattering terms without any loss of accuracy. This modifi-

cation of the ACOT scheme goes by the name Simplified-ACOT (S-ACOT) and can be summarized as follows.

S-ACOT: For hard-scattering processes with incoming heavy quarks or with internal on-shell cuts on a heavy quark line, the heavy quark mass can be set to zero ($m_Q = 0$) for these pieces [3].

If we consider the case of NLO DIS heavy quark production, this means we can set $m_Q = 0$ for the LO terms ($QV \rightarrow Q$) as this involves an incoming heavy quark, and we can set $m_Q = 0$ for the SUB terms as this has an on-shell cut on an internal heavy quark line. Hence, the only contribution which requires calculation with m_Q retained is the NLO $gV \rightarrow Q\bar{Q}$ process.

Figure 4 displays a comparison of a calculation using the ACOT scheme with all masses retained vs. the S-ACOT scheme; as promised, these two results match throughout the full kinematic region.

2.3. ACOT- χ

In the conventional implementation of the heavy quark PDFs, we must “rescale” the Bjorken x variable as we have a massive parton in the final state. The original rescaling procedure is to make the substitution $x \rightarrow x(1 + m_c^2/Q^2)$ which provides a kinematic penalty for producing the heavy charm quark in the final state [4]. As the charm is pair-produced by the $g \rightarrow c\bar{c}$ process, there are actually two charm quarks in the final

²While we have given a heuristic description of this result (in which we used some illustrative approximations), we emphasize the proof applies to all cases and does not require any such approximations.

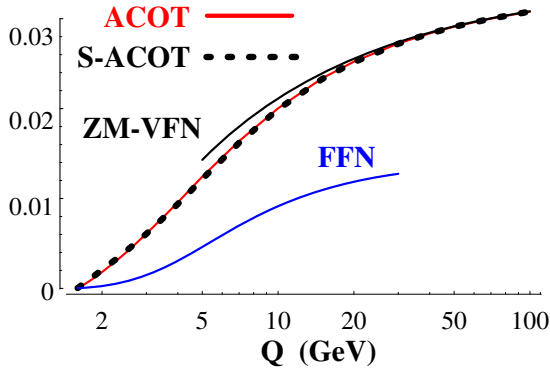


Figure 4. Comparison of schemes for NLO DIS heavy quark production as a function of Q . We display calculations using the ACOT, S-ACOT, Fixed-Flavor Number (FFN), and Zero-Mass Variable Flavor Number (ZM-VFN) schemes. The ACOT and S-ACOT results are virtually identical.

state—one which is observed in the semi-leptonic decay, and one which goes down the beam pipe with the proton remnants. Thus, the appropriate rescaling is not $x \rightarrow x(1 + m_c^2/Q^2)$ but instead $x \rightarrow \chi = x(1 + (2m_c)^2/Q^2)$; this rescaling is implemented in the ACOT- χ scheme, for example [5, 6, 7]. The factor $(1 + (2m_c)^2/Q^2)$ represents a kinematic suppression factor which will suppress the charm process relative to the lighter quarks.

2.4. Numerical Comparison

Having introduced the various theoretical issues which enter the calculation of the heavy quark process, we illustrate the numerical size of these choices for the case of DIS heavy quark production.

In Figure 5 we display the charm structure function $F_2^c(x, \mu)$ for a variety of schemes and orders. *LO* represents the $\mathcal{O}(\alpha_s^0)$ $QV \rightarrow Q$ process. *NLO* includes the $\mathcal{O}(\alpha_s^1)$ processes (primarily $gV \rightarrow QQ$) in the massless approximation. In the Fixed-Flavor-Scheme (FFS) the heavy quark PDF is set to zero; hence, at $\mathcal{O}(\alpha_s^1)$ this only receives contributions from $gV \rightarrow QQ$. The ACOT and S-ACOT schemes are virtually identical—the curves are indistinguishable in this plot. Finally,

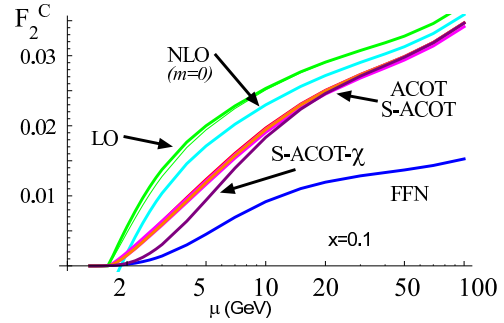


Figure 5. Calculation of DIS heavy quark production for a variety of schemes.

the implementation of the χ -prescription for the S-ACOT scheme (the ACOT- χ would yield identical results) provides some additional suppression in the region $\mu \sim m_Q$. To this order, our best theoretical estimate of the true cross section would be either the ACOT- χ or equivalently S-ACOT- χ .

To see the effect of these different results in the context of a global fit we display the results for the CTEQ6M and CTEQ6HQ PDFs sets in Table 1. Both the fits using a consistent application of the ACOT and \overline{MS} schemes yield good results. In contrast, if we mismatch the scheme used in the PDF with that in the cross section calculation we observe a dramatic increase in the χ^2 values obtained. This result underscores the importance of using properly matched calculations.

2.5. Heavy Quarks at the Tevatron

In the previous discussion we have primarily focused on DIS production of heavy quarks for illustrative purposes as the formalism is easier to layout when there is only a single hadron in the initial state. Nevertheless, the same principles that we have used in the DIS case can be applied to that of the hadron-hadron initial state as appropriate for the Tevatron and the LHC.

Historically, the predictions of b-production at hadron-hadron colliders have been a challenge; the early results from the Tevatron were a factor of 2 to 3 larger than the theoretical predictions. NLO QCD corrections to the LO $gg \rightarrow QQ$

Set	# points	CTEQ6HQ	CTEQ6M	6M \otimes GM	6HQ \otimes ZM
ZEUS	104	0.91	0.98	2.84	3.72
H1	484	1.02	1.04	1.50	1.22
TOTAL	1925	1.04	1.06	1.26	1.30

Table 1

Table of χ^2 per point for the individual HERA data sets, and for the TOTAL of all data sets. (Non-HERA data sets are not displayed.) The results are shown for CTEQ6HQ PDF using the General Mass (GM) ACOT scheme, and CTEQ6M PDF using the zero-mass (ZM) \overline{MS} scheme. We note the increased χ^2 for mixed schemes using CTEQ6M with the GM ACOT scheme, and the CTEQ6HQ with the ZM scheme.

process were formidable and yielded large corrections [8, 9, 10, 11, 12]. It is interesting to observe that if the heavy quark PDF is taken into account so that the LO contribution consists of both $gg \rightarrow QQ$ and $gQ \rightarrow gQ$, then the computed NLO contributions (with appropriate subtractions) are thereby reduced suggesting improved convergence of the perturbation theory [13, 14, 15, 16, 17, 18].

Ref. [19] performs a systematic comparison of the GM-VFNS and ZM-VFNS using results of an updated analysis of hadronic b-production at the Tevatron. Figure 6 displays these results for the Tevatron in the central rapidity region as compared with the CDF data [20, 21]. The result is that the finite mass effects moderately enhance the p_T distribution in the region $p_T \sim 2m_H$ by about 20%, and this enhancement decreases at larger p_T . For intermediate to large p_T values ($p_T > m_H$) the three calculations (GM-VFNS, ZM-VFNS, FFN) match quite closely, and are in good agreement with the data. Conversely, if we use the FFN result with the historic values for the PDF and α_S we find this prediction is roughly a factor of 3 below the data.

The excellent agreement between data and theory for this process is an important achievement and represents the culmination of many years of effort by both the theoretical and experimental community.

3. Schemes used for Global Analysis

The ACOT scheme and variants were used for the CTEQ series of global PDF fits.³ For the MRST/MSTW series of global PDF fits the

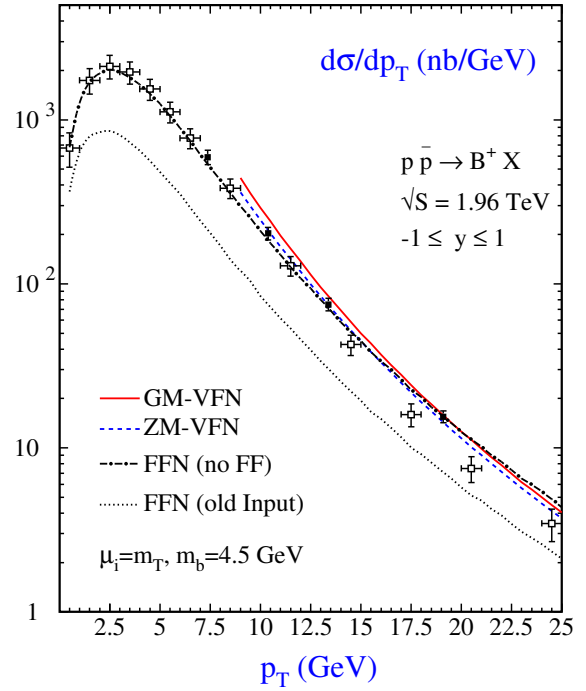


Figure 6. From Ref. [19], the transverse momentum distribution $d\sigma/dp_T$ for $p\bar{p} \rightarrow BX$ at $\sqrt{s}=1.96$ TeV. The results are shown for the General Mass (GM) Variable Flavor Number (VFN) scheme and the Zero Mass (ZM) Variable Flavor Number (VFN) scheme. Additionally, results are shown for the Fixed Flavor Number (FFN) scheme with both recent PDFs (dot-dashed line) and the historical PDFs (dotted line). The data is from the CDF collaboration [20, 21].

³Specifically, ACOT was used for CTEQ6HQ, and S-ACOT- χ was used in CTEQ6.5 and CTEQ6.6.

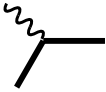
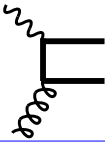
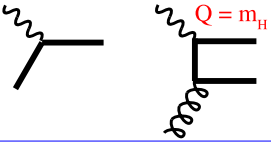
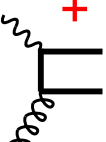
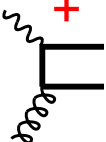
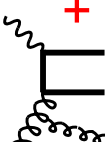
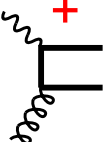
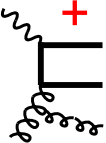
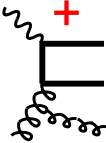

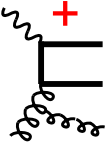
ACOT type schemes			TR type schemes		
	$Q < m_H$	$Q > m_H$ <small>constant term</small>		$Q < m_H$	$Q > m_H$ <small>constant term</small>
LO	\emptyset	 \emptyset	LO	 \emptyset	 $Q = m_H$
NLO	 $+$	 \emptyset	NLO	 $+$	 $Q = m_H$
NNLO	 $+$	 \emptyset	NNLO	 $+$	 $Q = m_H$

Figure 7. Diagrammatic comparison of TR and ACOT type schemes for the case of DIS. This diagram is schematic to emphasize the similarities and differences. The leading-order (LO) process is a $\mathcal{O}(\alpha_s^0)$ boson scattering from a heavy quark, e.g. $\gamma Q \rightarrow Q$; the NLO $\mathcal{O}(\alpha_s^1)$ correction arises from $\gamma g \rightarrow Q\bar{Q}$, and the NNLO $\mathcal{O}(\alpha_s^2)$ correction arises from $\gamma g \rightarrow Q\bar{Q}g$.

Thorne-Roberts (TR) scheme was used. As these two sets of PDFs are widely used it is of interest to compare and contrast these approaches. Figure 7 displays a diagrammatic comparison of the TR [22, 23] and ACOT type schemes. While these schemes may appear quite different at first glance, they differ by higher-order terms which will be reduced as we increase the order of our perturbation theory.

In perturbation theory, we compute our observables to a fixed order N in α_s ; hence, we truncate the perturbation expansion at $\mathcal{O}(\alpha_s^N)$, and we have neglected terms of order $\mathcal{O}(\alpha_s^{N+1})$. In brief, the difference between these two approaches amounts to adding different $\mathcal{O}(\alpha_s^{N+1})$ higher order terms. Thus, these two approaches will agree on the contributions up to $\mathcal{O}(\alpha_s^N)$. We will now review the motivation and consequences of adding the differing higher order terms.

3.1. Leading-Order (LO) (α_s^0)

If we work at Leading-Order⁴ (LO) α_s^0 , when the heavy quark PDF is an “active” parton (typically $\mu > m_H$) the LO contribution is $\gamma + Q \rightarrow Q$. However, when the heavy quark PDF is *not* an “active” parton (typically $\mu < m_H$) the LO contribution vanishes. For the ACOT scheme, no higher order terms are added to this results. Hence for scales $\mu < m_H$, the LO answer is zero and we expect large corrections to this result at NLO. For the TR scheme, a portion of the $\gamma g \rightarrow Q\bar{Q}$ contribution is added; for $\mu < m_H$ the full $\gamma g \rightarrow Q\bar{Q}$ term is included, and for $\mu > m_H$ the $\gamma g \rightarrow Q\bar{Q}$ term frozen at $\mu = Q = m_H$ to avoid any difficulty with large logarithms of the form $\ln(m_H/\mu)$.

Consequently, in the $\mu < m_H$ region the TR

⁴Here, we define the order of the calculation according to the power of α_s ; thus LO is α_s^0 , NLO is α_s^1 , etc.

scheme yields a finite LO result while the ACOT scheme yields zero. While both schemes formally agree at $\mathcal{O}(\alpha_S^0)$, clearly the $\mathcal{O}(\alpha_S^1)$ terms can be important, particularly in the $\mu < m_H$ region.

3.2. Next-to-Leading-Order (NLO) (α_S^1)

If we work at NLO (α_S^1), for the low μ region we now include $\gamma g \rightarrow Q\bar{Q}$ as well as the $\gamma + Q \rightarrow Q$ process.⁵ If we again look in the region $\mu < m_H$, we find that while the ACOT scheme yielded zero at LO, it now obtains a finite result at NLO. For the TR scheme, in addition to the above terms, a portion of the $\gamma g \rightarrow gQ\bar{Q}$ contribution is added; again, for $\mu > m_H$ the $\gamma g \rightarrow gQ\bar{Q}$ term is frozen at $\mu = Q = m_H$ to avoid any difficulty with large logarithms.

As before, both the TR scheme and ACOT scheme formally agree at $\mathcal{O}(\alpha_S^1)$, but they will differ by the separate NNLO $\mathcal{O}(\alpha_S^2)$ terms that have been included. In contrast to the LO case where the ACOT scheme yielded zero for $\mu < m_H$, both schemes give finite results in all kinematic regions; hence, the relative difference will be reduced.

3.3. General Comparisons at Order α_S^N

Let us make some observations regarding these schemes at a general order in perturbation $\mathcal{O}(\alpha_S^N)$. We observe that for a given set of processes calculated to α_S^N , we can implement the TR scheme to $\mathcal{O}(\alpha_S^{N-1})$ and the ACOT scheme to $\mathcal{O}(\alpha_S^N)$. For example, at NLO we note that the ACOT scheme involves only graphs of order α_S^1 while TR utilizes graphs of order α_S^2 . At present we know the $\mathcal{O}(\alpha_S^2)$ massive neutral current process ($\gamma g \rightarrow gQ\bar{Q}$, $\gamma Q \rightarrow ggQ$ and associated graphs); hence, this allows us to compute the TR scheme to $\mathcal{O}(\alpha_S^1)$ and the ACOT scheme to $\mathcal{O}(\alpha_S^2)$. In contrast, the massive charged current process is known only to $\mathcal{O}(\alpha_S^1)$; hence, this allows us to compute the TR scheme to $\mathcal{O}(\alpha_S^0)$ and the ACOT scheme to $\mathcal{O}(\alpha_S^1)$.

We note that recent improvements of theoretical techniques have enabled significant advances in the calculation higher-order heavy quark pro-

cesses. For example, Ref. [25] has obtained the asymptotic results for $F_L^{Q\bar{Q}}(x, \mu)$ at the 3-loop order, and recently Ref. [26] has extended this work for the case of $F_2^{Q\bar{Q}}(x, \mu)$.

In general, the TR scheme achieves in practice the same highest asymptotic order as ACOT by some modeling of terms below $Q^2 = m_Q^2$ which become (relatively) unimportant at high Q^2 . As we move to higher order calculations, the differences between these schemes will be reduced as they arise from uncalculated higher-order contributions.

4. NNLO and Beyond

Although NLO is the state-of-the-art for many calculations, improved experimental precision demands that we strive toward a NNLO accuracy. When we consider PDFs for heavy quarks at NNLO, there are a number of new elements that enter.

One consequence is that the PDFs are no longer continuous across the heavy flavor threshold. Even more, when matching charm and bottom across their thresholds, they start from negative values as illustrated in Figure 8. The matching conditions have been computed by a number of groups [27, 28], and at NNLO PDFs will have

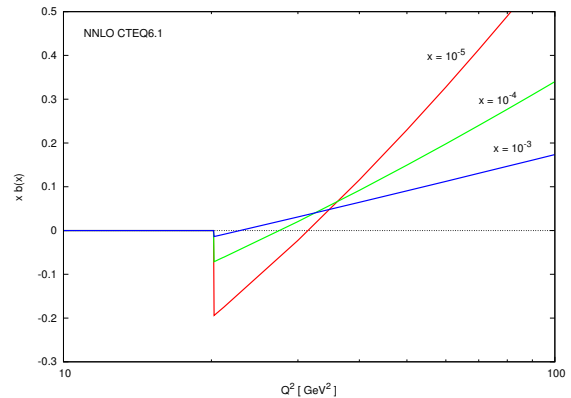


Figure 8. The b-quark PDF $x f_b(x, Q)$ with NNLO matching conditions for 3 choices of x .

⁵Note, in Figure 7 and in the discussion the diagrams and processes are schematic and illustrative. For example, at NLO we include both $\gamma Q \rightarrow Qg$ and $\gamma g \rightarrow Q\bar{Q}$ as well as all the corresponding subtractions. For details see Refs. [22, 24].

discontinuities of order $\mathcal{O}(\alpha_S^2)$ when we transition from N_F to $N_F + 1$ flavors. While we may be uncomfortable with discontinuities in our PDFs, we are reminded that the PDFs are not physical observables, but instead are only theoretical constructs which depend on (arbitrary) renormalization schemes and scales.⁶

At NLO, the point $\mu = m_Q$ is special because $f_a^{N_F}(x, m_Q) = f_a^{N_F+1}(x, m_Q)$; this is because the constant term in the matching equation happens to be zero at NLO. Because of this “accident” it was common to use $\mu = m_Q$ as both the Matching Point and the Transition Point.

At NNLO the point $\mu = m_Q$ no longer has these special properties as the transition from N_F to $N_F + 1$ will necessarily have discontinuities at any value of μ ; hence, it may be desirable to choose the Matching Point and the Transition Point at different values of μ . As these two point are not usually distinguished, let us highlight their features.

Matching Point μ_M : The value of μ where the $N_F + 1$ scheme is defined in terms of the N_F scheme by a relation of the form: $f_a^{N_F+1}(x, \mu) = A_{ab} \otimes f_b^{N_F}(x, \mu)$.

Transition Point μ_T : The value of μ where the user chooses to transition from the N_F scheme to the $N_F + 1$ scheme.

Figure 9 schematically represents how each calculation with a set number of flavors N_F has a particular region of applicability where it is best suited to describe the “true” physics. The complete description of the physics throughout the full kinematic range will therefore consist of a patchwork of schemes which are “sewn together.”

The Transition Point: It is easy to imagine situations where we would not want to automatically transition between schemes at $\mu = m_Q$. For example, consider we are analyzing data in the range $\mu \in [2, 5]$ GeV. The bulk of the range is in the $N_F = 4$ flavor region as $\mu > m_c \sim 1.3$ GeV,

⁶Recall $\alpha_S(\mu)$ is also an unphysical theoretical construct; this has discontinuities across flavor-thresholds at order α_S^3 .

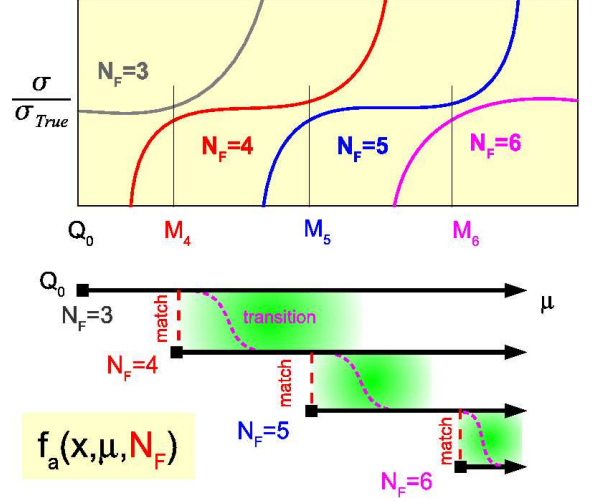


Figure 9. The upper figure schematically represents how each calculation with a set number of flavors N_F has a region of applicability. The transition from the N_F-1 scheme to the N_F scheme should be in the vicinity of the m_{N_F} mass, but need not occur exactly at $\mu = m_{N_F}$. The lower figure illustrates that multiple PDFs can co-exist for $\mu \geq m_{N_F}$ with matching performed at $\mu = m_{N_F}$.

but a small portion of the range extends above the $N_F = 5$ flavor region as $\mu > m_b \sim 4.5$ GeV. In the region $\mu \in [4.5, 5]$ GeV it would be inconvenient to be forced to transition to a $N_F = 5$ scheme because 1) the b-quark clearly plays no substantive role in this kinematic range, and 2) both the PDFs and $\alpha_s(\mu)$ will have discontinuities at $\mu = m_b$.

Clearly it is more reasonable to have the option to work consistently in a $N_F = 4$ flavor scheme even for $\mu \gtrsim m_b$. If PDFs were generated such that the $N_F = 4$ and $N_F = 5$ schemes co-exist in the region $\mu \sim m_b$, then the user could select N_F by choice.

The lower portion of Figure 9 illustrates how this might be implemented. The PDFs can be generated such that the N_F scheme is available for all $\mu \geq m_{N_F}$. Thus, for $\mu = 5$ GeV the user

would have access to schemes with $N_F = \{3, 4, 5\}$ and can select the scheme by specifying N_F in addition to $\{x, \mu\}$. Therefore, the user could analyze their $\mu \in [2, 5]$ GeV data set consistently in a single $N_F = 4$ scheme, and choose to transition to the $N_F = 5$ scheme at a higher μ value to be specified by the user.

The Matching Point: Although the Matching Point can be set to any μ value in the region of m_{N_F} , we shall argue that the choice $\mu_M = m_{N_F}$ is optimal.

First, we note that the Matching Point should be at or below the Transition Point ($\mu_T \geq \mu_M$) if we desire to avoid downward DGLAP evolution (which can be unstable). Therefore, if we perform the matching at the heavy quark mass we have the reasonable constraint: $\mu_T \geq \mu_M = m_{N_F}$.

Second, the matching conditions which define $f_a^{N_F+1}$ in terms of $f_a^{N_F}$ are of the form $f_a^{N_F+1} = A_{ab} \otimes f_b^{N_F}$ with

$$A_{ab} = \delta_{ab} + \frac{\alpha_s}{2\pi} P_{b \rightarrow a} \left[\ln \left(\frac{\mu^2}{m_Q^2} \right) + c_{b \rightarrow a} \right]$$

up to $O(\alpha_s^2)$. Here, $P_{b \rightarrow a}$ is the DGLAP splitting kernel and $c_{b \rightarrow a}$ is a constant.⁷ The choice $\mu_M = m_{N_F}$ eliminates the logarithmic terms thus simplifying the calculation.

We also observe that shifting the Matching Point from m_Q to $2m_Q$ does not suppress the heavy quark PDF as the logarithmic terms compensate for evolution between m_Q and $2m_Q$.

5. Conclusions:

The computation of heavy quark production has historically been challenging both theoretically and experimentally. On the theoretical side, the heavy quark introduces an additional mass scale which complicates the calculations. On the experimental side, the data for heavy quark production has typically differed from the theoretical

predictions by a significant factor. Recent theoretical developments enable us to incorporate the heavy quark mass into the calculation both dynamically and kinematically. These calculations have been used to produce matched PDFs incorporating the full mass dependence. Updated analyses show improved agreement between data and theory for both HERA and Tevatron measurements.

Improved experimental precision will demand NNLO accuracy from the theoretical calculations, and this introduces a number of issues not present at the NLO order. There is progress underway on both the PDFs and the hard-scattering calculations, and this should ensure we are well prepared for the upcoming LHC data.

Acknowledgments: We would like to thank John Collins, Gustav Kramer, Stefan Kretzer, Pavel Nadolsky, M.H. Reno, Davison Soper, Robert Thorne, Wu-Ki Tung, Ji Young Yu, for valuable discussion. F.I.O. acknowledges the hospitality of CERN, DESY, and the Université Joseph Fourier, Grenoble where a portion of this work was performed. This work was partially supported by the U.S. Department of Energy.

REFERENCES

1. J.C. Collins, "Hard-scattering factorization with heavy quarks: A general treatment," Phys. Rev. D **58** (1998) 094002.
2. F.I. Olness and R.J. Scalise, "Heavy quark parton distributions: Mass dependent or mass independent evolution?," Phys. Rev. D **57** (1998) 241.
3. M. Krämer, F.I. Olness and D.E. Soper, "Treatment of heavy quarks in deeply inelastic scattering," Phys. Rev. D **62** (2000) 096007.
4. R.M. Barnett, "Evidence for New Quarks and New Currents," Phys. Rev. Lett. **36** (1976) 1163.
5. J. Amundson, F.I. Olness, C. Schmidt, W.-K. Tung and X. Wang, "Theoretical description of heavy quark production in DIS," Proc. of DIS 98, Brussels, Belgium, 4-8 Apr (1998).
6. J. Amundson, C. Schmidt, W.-K. Tung and X. Wang, "Charm production in deep inelastic

⁷The matching conditions are determined entirely by the DGLAP evolution kernels up to a constant term which must be computed. At NLO, the constant term is zero such that the PDFs are continuous; at NNLO, this term is non-zero.

- scattering from threshold to high Q^2 ,” JHEP **10** (2000) 031.
7. W.-K. Tung, S. Kretzer and C. Schmidt, “Open heavy flavor production in QCD: Conceptual framework and implementation issues,” J. Phys. G **28** (2002) 983.
 8. P. Nason, S. Dawson and R.K. Ellis, “The Total Cross-Section for the Production of Heavy Quarks in Hadronic Collisions,” Nucl. Phys. B **303** (1988) 607.
 9. G. Altarelli, M. Diemoz, G. Martinelli and P. Nason, “Total Cross-Sections for Heavy Flavor Production in Hadronic Collisions and QCD,” Nucl. Phys. B **308** (1988) 724.
 10. W. Beenakker, H. Kuijf, W.L. van Neerven and J. Smith, “QCD Corrections to Heavy Quark Production in p anti-p Collisions,” Phys. Rev. D **40** (1989) 54.
 11. P. Nason, S. Dawson and R.K. Ellis, “The One Particle Inclusive Differential Cross-Section for Heavy Quark Production in Hadronic Collisions,” Nucl. Phys. B **327** (1989) 49.
 12. W. Beenakker, W.L. van Neerven, R. Meng, G.A. Schuler and J. Smith, “QCD corrections to heavy quark production in hadron hadron collisions,” Nucl. Phys. B **351** (1991) 507.
 13. M. Cacciari and M. Greco, “Large P_T hadroproduction of heavy quarks,” Nucl. Phys. B **421** (1994) 530.
 14. F.I. Olness, R.J. Scalise and W.-K. Tung, “Heavy quark hadroproduction in perturbative QCD,” Phys. Rev. D **59** (1999) 014506.
 15. M. Cacciari, M. Greco and P. Nason, “The P_T spectrum in heavy-flavour hadroproduction,” JHEP **05** (1998) 007.
 16. M. Cacciari, S. Frixione and P. Nason, “The P_T spectrum in heavy-flavor photoproduction,” JHEP **03** (2001) 006.
 17. M. Cacciari and P. Nason, “Is there a significant excess in bottom hadroproduction at the Tevatron,” Phys. Rev. Lett. **89** (2002) 122003.
 18. M. Cacciari, S. Frixione, M.L. Mangano, P. Nason and G. Ridolfi, “QCD analysis of first b cross section data at 1.96-TeV,” JHEP **07** (2004) 033.
 19. B.A. Kniehl, G. Kramer, I. Schienbein and H. Spiesberger, “Finite-mass effects on inclusive B-meson hadroproduction,” Phys. Rev. D **77** (2008) 014011.
 20. A. Abulencia *et al.*, “Measurement of the B+ production cross section in p anti-p collisions at $\sqrt{s} = 1960$ GeV,” Phys. Rev. D **75** (2007) 012010.
 21. D.E. Acosta *et al.*, “Measurement of the J/ψ meson and b -hadron production cross sections in $p\bar{p}$ collisions at $\sqrt{s} = 1960$ GeV,” Phys. Rev. D **71** (2005) 032001.
 22. R.S. Thorne, “A variable-flavour number scheme for NNLO,” Phys. Rev. D **73** (2006) 054019.
 23. R.S. Thorne, “Heavy quarks in MRST/MSTW global fits,” Contribution to these proceedings (2008).
 24. M.A.G. Aivazis, J.C. Collins, F.I. Olness and W.-K. Tung, “Leptoproduction of heavy quarks. II. A Unified QCD formulation of charged and neutral current processes from fixed target to collider energies,” Phys. Rev. D **50** (1994) 3102.
 25. J. Blumlein, A. De Freitas, W.L. van Neerven and S. Klein, “The longitudinal heavy quark structure function $F_L^{Q\bar{Q}}$ in the region $Q^2 \gg m^2$ at $\mathcal{O}(\alpha_s^3)$,” Nucl. Phys. B **755** (2006) 272.
 26. I. Bierenbaum, J. Blumlein and S. Klein, “First $\mathcal{O}(\alpha_s^3)$ heavy flavor contributions to deeply inelastic scattering,” Nucl. Phys. Proc. Suppl. **183** (2008) 162.
 27. M. Buza, Y. Matiounine, J. Smith, R. Migneron and W.L. van Neerven, “Heavy quark coefficient functions at asymptotic values $Q^2 \gg m^2$,” Nucl. Phys. B **472** 1996 611.
 28. M. Cacciari, P. Nason and C. Oleari, “Crossing heavy-flavour thresholds in fragmentation functions,” JHEP **10** (2005) 034.